Journal Title
XX(X):1–??

DOI: 10.1177/ToBeAssigned
www.sagepub.com/
SAGE

Numerical modelling and vibration serviceability assessment of a steel footbridge with a significant 3D dynamic behaviour

Victor Roda-Casanova[1], David Hernández-Figueirido[1], Joaquín L. Sancho Bru[1] and Maria D. Martínez-Rodrigo[1]

Abstract

This paper focuses on the vibration serviceability assessment and numerical modelling of an existing steel truss footbridge located in the outskirts of Castellón, Spain. The footbridge is rather slender and composed by a main span and two access ramps supported on three four-arm piers of different heights. Due to the connection between the main span and the ramps at the top of the the tall piers, longitudinal and lateral bending/torsion natural coupled modes of vibration coexist at low frequencies, with a relevant contribution of the piers and access ramps deformation. This leads to a significant three-dimensional and rather complex dynamic response under service conditions. With the aim of characterising the structural dynamic properties and assessing the level of vibrations induced by crossing pedestrians, two in-situ experimental test programs are conducted. On the one hand, the structural response is measured during several hammer tests and the modal properties are identified and used to update a detailed 3D numerical model by means of a Genetic Algorithm. Due to the lack of information regarding the detailing of the piers foundations, two alternative models are analysed. The relevance of the pier-foundation system rotational stiffness is highlighted for the particular configuration. On the other hand, the footbridge main span response is recorded under different pedestrian activities: walking, running and vandal simulated actions. Finally, the vibration serviceability of the structure is assessed based on current codes and regulations.

Keywords

Footbridges, Numerical modelling, Experimental testing, Modal identification, Vibration serviceability

Introduction

Pedestrian footbridges are rather slender and flexible structures with relatively high live-load to self-weight ratios. Such structures usually present the lowest natural frequencies in the range of the loading frequencies of human-induced excitation. Additionally, when built with steel or composite materials, footbridges may exhibit relatively low damping levels. For the above reasons, these structures can easily be stimulated to vibrate when pedestrians walk or run across them, and it becomes essential to assess their serviceability in order to ensure the safety and comfort of the users (1). Vibration phenomena in footbridges is generally a serviceability concern, as human perceives very small vibration amplitudes, far below those leading to damage (2; 3). In the last decades, excessive vibration problems have been detected in some famous pedestrian footbridges, e.g. Millenium Bridge in London, Pasarelle Solferino in Paris or Toda Park Bridge in Saitama, Japan (4; 5).

Design guidelines and regulations of different countries address the serviceability limit state associated to human-induced vibrations in footbridges (6; 7; 8; 9; 10; 11). In general, in all these sources excitation frequency ranges associated to different pedestrian actions are defined, and these actions effects on footbridges are discussed by differentiating the vertical and longitudinal from the lateral response, with respect to the crossing direction. When the lowest natural frequencies of the structure fall in the pedestrian excitation frequency range, dynamic analyses should be carried out to verify the comfort criteria. These guidelines present some shortcomings. First, they admit that the footbridge dynamic response is caused by resonance of a single mode excited by the pedestrian action. However, footbridges usually present close modes at low frequencies which may be simultaneously excited (12). Second, they disregard human-structure interaction effects. Recent studies have shown that the effective damping introduced by the pedestrian action may be higher than the modal damping identified on the empty bridges (13). This is specially relevant in the vertical direction, while in the lateral one, the lock-in phenomenon may build up, leading to high accelerations with the synchronisation of the pedestrian step frequencies (14). Third, they also ignore human-human interaction and how the behaviour of each pedestrian is affected by the crowd (15).

[1]Department of Mechanical Engineering and Construction, Universitat Jaume I, Spain

Corresponding author:
Victor Roda-Casanova, Department of Mechanical Engineering and Construction, Universitat Jaume I, Spain.
Email: vroda@uji.es

Some recent studies are devoted to the vibration serviceability assessment of particular case studies. In (16) the vibration serviceability and pedestrian comfort are evaluated on a curved lightweight footbridge in Jordan, by means of an experimental program. Tadeu et al. (17) investigate the vibrations induced by humans through in situ behaviour tests on the Arouca footbridge in Portugal, world's longest span in 2020 suspended footbridge. The authors underline the amplitude dependence of the identified damping ratios, and complement the assessment of pedestrian comfort with surveys filled in by the visitors. Bayat et al. (18) identify the modal parameters and analyse the state of degradation and the level of vibrations of a historic suspension footbridge under the action of a single pedestrian through low-cost non-invasive dynamic testing. Rodriguez-Suesca et al. (19) assess the dynamic characteristics and dynamic performance of eight deteriorating footbridges in Colombia following a numerical-experimental approach. The authors show an unsafe level of vibrations in most of the structures for temporary and exceptional loading conditions, and compare discomfort and deterioration levels using specific indices. In short, there are numerous structures that, due to their typology and dimensions, material, slenderness or state of preservation, may experience significant vibration levels under normal conditions of use. It is therefore essential (i) to be able to predict the dynamic behavior in the design phase, progressing in the numerical modelling techniques, and (ii) to assess the footbridges performance in the case of existing structures or under new conditions of use, improving experimental procedures. This work contributes to the current knowledge on these two aspects.

Some mechanisms that give rise to the human-induced vibration problem in footbridges are still under investigation. That is the case of the amplification in the lateral vibrations due to the synchronisation among the pedestrians and the structure, also known as *lock-in* phenomenon. Andrade et al. (20) investigate experimentally the conditions that could lead to the avoidance of this type of synchronisation. Cuevas et al. (21) propose a general formulation which allows the analysis of the different load scenarios that the footbridge will experience during its overall life cycle. The procedure permits the evaluation of the comfort level even with crowd densities above the critical number and thus, to evaluate the footbridge comfort once the lock-in effect has initiated.

In the need to improve the dynamic behavior of these structures, some recent studies deal with the application of passive or semi-active control techniques. Gallegos-Calderón et al. (22) present the design of a passive inertial controller to be installed on an ultralight-weigth fiber-reinforced footbridge. Saber et al. (23) compare the retrofit of a footbridge experiencing frequency variations over time and under walking pedestrians with semi-active and classical passive dynamic vibration absorbers. Zoltowski et al. (24) present the structural modification of a pedestrian drawbridge to raise its fundamental bending frequency to a level where pedestrian action has a low influence by introducing a high coefficient passive damper.

In this context, being able to realistically predict the structures modal parameters, their alteration with use and environmental conditions, and adequately characterizing and simulating human action becomes a priority. Regarding the characterisation of pedestrian action, Van Nimmen et al. (13) introduces a methodology that uses registered body motion to reconstruct the vertical dynamic running load. Pfeil et al. (25) propose a biodynamic model based on the single-degree-of-freedom (SDOF) system subjected to base excitation. In line with the variability of the structural parameters and the need to characterize the dynamic behavior of the structure realistically, effort is currently being devoted to the investigation of temperature effects on the footbridges modal parameters (26), and on how to discern those from damage-related variations (27).

In the present work the dynamic response of an existing steel truss footbridge is evaluated after detecting relevant vertical and lateral vibrations on its main span. The structural configuration leads to an important participation of three-dimensional modes. Also, due to the shared high piers supports, the three parts conforming the structure (two access ramps and the main span) interact in such a way that stating in advance the best modelling alternative is not a straight forward matter. As an added and rather common difficulty the information available on the structure is scarce.

The paper is organised as follows: first, relevant information found in the design codes and guidelines on the vibration serviceability assessment of footbridges is summarised; second, the footbridge under study is described; third, two experimental programs performed with the aim of identifying the bridge modal parameters and assessing the level of vibrations under different human actions, including those associated to vandalism, are presented. Fourth, a detailed finite element (FE) numerical model is implemented and updated from the experimental data. After detecting the high influence of the piers deformability and of the boundary conditions, two modelling alternatives are evaluated. Finally, the dynamic performance of the footbridge is assessed numerically according to standards. In the last section, the main findings are summarised and conclusions and future developments are stated.

Vibration serviceability in footbridges. Current codes of practice

Current codes and guidelines used in different countries for vibration serviceability limit states of footbridges are briefly presented in this section. The vibration serviceability of footbridges is based on the human comfort level, which is assessed through reference to the acceleration undergone by the structure. Additionally, the codes and recommendations establish frequency ranges of the footbridges natural frequencies to predict the risk of resonance induced by pedestrians, and the need to perform dynamic analyses to verify the comfort criteria.

Frequency ranges to assess the risk of resonance. Tab. 1 provides a summary of the frequency ranges offered by different codes associated to high risk of resonance for vertical and longitudinal vibrations, on one hand, and for lateral horizontal vibrations, on the other. Some codes provide two ranges for vertical vibrations, corresponding to resonance excited by the 1st or 2nd harmonic of pedestrian action. Lateral vibrations are no affected by the 2nd harmonic. The most recent and widely applied in practice guides are

the European guidelines HiVoSS (8) and Setra (7). These guidelines provide four frequency ranges corresponding to a decreasing risk of resonance (see Figs. 1a-b). These ranges will be referred to in the upcoming sections.

Table 1. High risk of resonance frequency limits for vertical and lateral vibrations according to different codes.

Codes of practice	Harm. #	Vertical (Hz)	Lateral (Hz)
Eurocode 0. A2 (6)	1	$1.60 - 2.40$	$0.80 - 1.20$
Setra (2006) (7)	1	$1.00 - 2.60$	$0.30 - 1.30$
	2	$2.60 - 5.00$	
Hivoss (2007 (8)	1	$1.25 - 2.30$	$0.50 - 1.20$
	2	$2.50 - 4.60$	
IAP-11 (2011) (9)	1	$1.25 - 4.60$	$0.50 - 1.20$
BS5400 (10)	1	< 5.00	< 1.50
LFRD (2020) (11)	1	< 3.00	

Acceleration limits for footbridges. Criteria for pedestrian comfort are most commonly represented as a limiting acceleration for the footbridge in the vertical and lateral directions. The limits established by Eurocode 0 (6), in Annex A2.4.3.2, for any part of the deck, are 0.7 m/s^2 for vertical vibrations, 0.2 m/s^2 for horizontal vibrations under normal use, and 0.4 m/s^2 for exceptional crowd conditions. HiVoSS and Setra apply the same criteria for pedestrian comfort (see Fig. 1c), which also match the recommendations by the Spanish Standard IAP-11 (9) for road bridge and footbridge design.

Damping ratios for service loads. Damping mechanisms in footbridges depend on the structure materials, configuration, construction details, bearing conditions, among other factors. HiVoSS and Setra adopt CEB information bulletin No. 209 (28) and recommend the values included in Tab. 2 in the design phase. In the same table, the ratios suggested in Spanish Standard IAP-11 are included as well. The values are rather consistent, and a common 0.4% is recommended for a steel footbridge as the one analysed in this paper. Nonetheless, intentional loads can produce large levels of oscillations in light footbridges, which can lead to higher damping ratios. HiVoSS recommends 2.0% for steel welded footbridges in those scenarios.

Table 2. Average damping ratios (%) according to construction material for serviceability conditions.

Material	HiVoSS	Setra	IAP11
Reinforced concrete	1.30	1.30	1.50
Prestressed concrete	1.00	1.00	1.00
Steel	0.40	0.40	0.40
Composite steel-concrete	0.60	0.60	0.60
Timber	1.50	3.00	−−

Footbridge under study: structure description

The structure under study is a steel truss footbridge located in the outskirts of Castellón, Spain, (4001'54.8"N 004'58.7"W). It allows pedestrian and cyclist crossing of CV10 four line highway. The footbridge, which was

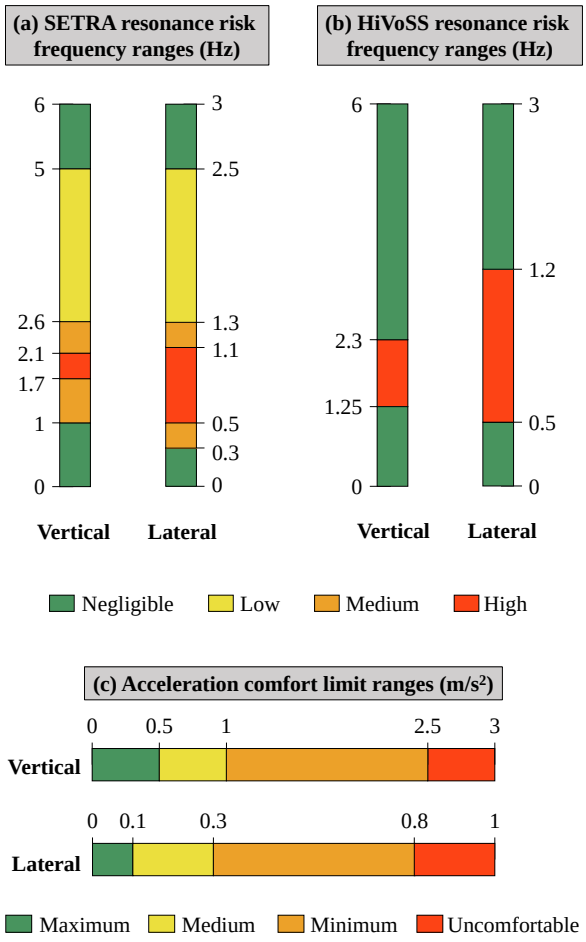

Figure 1. Levels or resonance risk associated to different vertical and lateral frequency ranges according to: (a) Setra and (b) HiVoSS. (c) Comfort levels associated to vertical and lateral acceleration ranges according to Setra and HiVoSS.

prefabricated and mounted in place, consists of a steel truss main span (see Fig. 2c) supported on two four-arm piers which land on rectangular concrete bases (see Fig. 2a), and two steel truss access ramps, from now on the North-West and the South-East ramps (see Fig. 7). The upper and lower chords of the trusses and the diagonal elements present rectangular hollow sections. The footbridge deck, identical in the three parts, consists of a 2.5 m wide steel plate supported on rectangular hollow longitudinal stringers and transverse beams. The dimensions of the structural members composing the super-structure are included in Fig. 2. The South-East ramp is simply supported on an abutment and connected to the south end of the main span. The North-West ramp rests on an intermediate four-arm pier between the north abutment and the connection to the main span (see Fig. 7). The four-arm piers are composed by variable section rectangular hollow tubes that converge on a vertical steel rectangular hollow base supported on reinforced concrete columns. The steel for the tubular profiles in the trusses and the steel used for the decks and the supports are most likely S275JR UNE EN10219 (29) and S275JR UNE EN10025 (30), respectively. The structure geometry was identified during field measurements since no technical information was available regarding the dimensions, materials nor construction detailing of any kind.

Specially relevant in this sense is the practical materialisation of the piers base embedment into the concrete columns (see Fig. 8) and the columns foundation itself. Moreover, the thickness of the four-arm piers cold-formed plates is admitted as 5 mm but it was not possible to validate this value by in-situ inspection. These uncertainties justify some of the decisions made in the model updating phase.

Experimental programs

In February 2021 and March 2022 the authors carried out two experimental programs on the footbridge with the aim of characterising the structure dynamic properties (Program #1) and assessing the vibration serviceability under pedestrian actions (Program #2). In this section the experimental program and the main results derived from it are presented.

Experimental setup

As per the acquisition equipment (see Fig. 2b) an 8-channel portable acquisition module LAN-XI type 3058 of Brüel & Kjær was used. The acquisition system fed the sensors (accelerometers). It also performed the Analog/Digital conversion (A/D). The A/D was carried out at a high sampling frequency that avoided aliasing effects using a low-pass filter with a constant cut-off frequency. The acquisition equipment was connected to a laptop for data storage. Bruel & Kjær model 8340 piezoelectric accelerometers were installed with a nominal sensitivity of 10000 mV/g and a lower frequency limit of approximately 0.1 Hz. The accelerometers were fixed to the bridge on magnetic mounting bases. The acquisition system was configured to avoid sensor overload.

Program #1: Identification of modal parameters. The experimental program for the identification of the footbridge modal parameters consisted in five impact hammer tests performed on the main span. Due to the limited number of sensors the tests were conducted in two different configurations, from now on configurations #1 and #2. The sensor layout and impact locations are shown in Fig. 3. Only the main span was instrumented. Notice that x, y and z refer to the longitudinal (crossing path), lateral and vertical directions with respect to the main span.

- In configuration #1, 7 accelerometers (A1z to A7z) were installed on the floor plate, at both sides of the deck measuring in the vertical direction; and 1 accelerometer was installed to measure longitudinal vibrations (A8x) in the connection area of the steel plate with the South-East access ramp. Excitation of the footbridge was carried out by hitting with a (non-instrumented) nylon hammer in the z-axis on three different spots of the deck plate identified as P1z to P3z in Fig. 3, so as to ensure exciting the main vertical bending and torsional modes of vibration.
- In configuration #2, all sensors were installed measuring in the lateral direction (y). Six of them were uniformly distributed along the bottom chord of the North-East vertical truss (A1y to A6y), and 2 of them were installed on the upper chord of each truss on each side of the main deck (A7y and A8y). Two excitation spots were considered in this case and the force was applied in the lateral (y) direction (P4y and P5y in Fig. 3).

Three impact tests took place per excitation spot to ensure test repeatability. The recorded signals, sampled at 512 Hz, were then post-processed applying third-order Chebyschef high pass (0.1 Hz) and low pass (30 Hz) filters to limit the analysis to the frequency range of interest. Cross Power Spectral Density was then applied to identify the natural frequencies and mode shapes, considering A4z and A4y as reference sensors for configurations #1 and #2, respectively. Fast Fourier Transforms (FFT) were also computed in order to estimate the damping coefficients using the Half-Power Bandwidth method.

Program #2: Vibration serviceability assessment. Fourteen tests were conducted on the footbridge to simulate various types of use by one and three pedestrians: walking, running at different speeds, and skipping/bouncing at specific frequencies, simulating a deliberate vandal actions. The tests are summarised in Tab. 3. For the walking test, three pedestrians walked randomly from one side to the opposite of the main span in circles. For the running tests, either one or three closely-spaced pedestrians crossed the main span from the South-East to the North-West ends. For the vandal tests one or three participants skipped or bounced at the center of the main span. The pace set was controlled by one operator carrying a digital metronome at the head of the line, in order to force pedestrians synchronisation at pre-defined frequencies. The excitation frequencies were selected in order to excite the natural frequencies identified in experimental Program #1, therefore either coinciding or being submultiples of them. In Tab. 3 for each test identified by the variable Test ID, successive columns stand for the number of pedestrians, their total mass, the test activity, the pace in beats per minute (bpm), the excitation frequency, the bridge frequency target harmonic and the test duration.

In Program #2, 8 accelerometers were placed at points of maximal amplitude of the vertical and lateral modes, identified from Program #1 impact tests, four of them measuring in the vertical direction (A1z to A4z), and the other four measuring in the lateral direction (A5y to A8y), as shown in Fig. 3 (Configuration #3).

Table 3. Serviceability assessment tests.

Test ID	Ped.	Mass (kg)	Activity	Pace (bpm)	Exc. Freq. (Hz)	Harm. #	Time (s)
1	1	60	Run	195	3.25	1	33
2	1	60	Run	128	4.26	2	38
3	1	60	Run	150	5.0	2	39
4	1	60	Run	155	7.74	3	33
5	1	60	Skip	195	3.25	1	49
6	1	60	Bounce	195	3.25	1	83
7	3	185	Walk	Rand	-	-	308
8	3	185	Run	195	3.25	1	92
9	3	185	Run	128	4.26	2	74
10	3	185	Run	150	5.0	2	75
11	3	185	Run	155	7.74	3	71
12	3	185	Skip	195	3.25	1	96
13	3	185	Bounce	195	3.25	1	91
14	3	185	Skip	150	5.00	2	118

Figure 2. Footbridge under study.

Experimental results

Program #1: Identification of modal parameters. The response of the structure to the impact tests performed for the identification of modal parameters is shown in Fig. 4, in the frequency domain, for two accelerometers in each configuration. The peaks corresponding to the natural frequencies of the structure can be clearly identified. Table 4 summarises the natural frequencies, mode shapes and modal damping ratios identified below 10 Hz. The mean value and standard deviation are included for the damping ratios. The fundamental frequency is 3.25 Hz, and the recorded amplitudes correspond to the first lateral mode of vibration of the main span. A further analysis of the numerical results presented later on shows that this deformation is accompanied by lateral bending of the North-West ramp with relevant participation of the supports (see Fig. 10a). The first vertical bending mode of the main span is observed at 5 Hz (Fig. 10c). Therefore, the lowest natural frequencies, both lateral and vertical, fall within the acceptable limits according to the European guidelines HiVoSS and SETRA (Figs. 1a and 1b). In the second, fourth and sixth modes the main span deforms under torsion. Numerical results help to distinguish that whereas for 4.25 Hz the deformation concentrates at the main span (Fig. 10b), for 7.75 Hz the access ramps also deform under torsion with relevant participation of the supports (Fig. 10d). At 9.25 Hz (Fig. 10f) the main span experiences second torsion along with first torsion of the South-East ramp. Finally, the fifth mode only shows significant contribution from the accelerometers located on the upper chords of both trusses, moving laterally in opposition. The level of vibrations recorded in the longitudinal direction (A8x) was marginal in all tests, with highest amplitudes associated to frequencies 4.25 Hz and 5 Hz.

The level of damping identified for the fundamental mode, 1.46%, exceeds the 0.4% recommended value for steel footbridges under service loads (see Table 2) and is lower than the level prescribed for large amplitudes of vibration 2.0%, according to (8). The (moderate) dispersion of the damping ratios identified experimentally aims to the difficulties for estimating this parameter accurately and to its amplitude-dependence.

Table 4. Modal parameters identified in the experimental program.

Freq. (Hz)	Modal shape at main span	Observed in config. #	Damping ratio (%) Mean	SD
3.25	Lateral bending	1 & 2	1.461	0.855
4.25	Torsion	1 & 2	1.090	0.667
5.00	Vertical bending	1	0.832	0.255
7.75	Torsion	1 & 2	0.787	0.701
8.56	Truss local bending	1 & 2	0.509	0.242
9.25	Torsion	1 & 2	0.848	0.437

Program #2: Assessment of the serviceability limit state. The dynamic analysis of the structural response to pedestrian use and vandal loading is presented in this section. The analysis of vandal loading covers the pedestrian skipping and bouncing tests, aimed to excite the natural modes in all directions, but particularly in the lateral and vertical directions. As previously mentioned, the lowest natural frequencies identified from Program #1 in the lateral and vertical directions (3.25 and 5 Hz) fall within the ranges of minimum resonance risk. Nevertheless, during the program

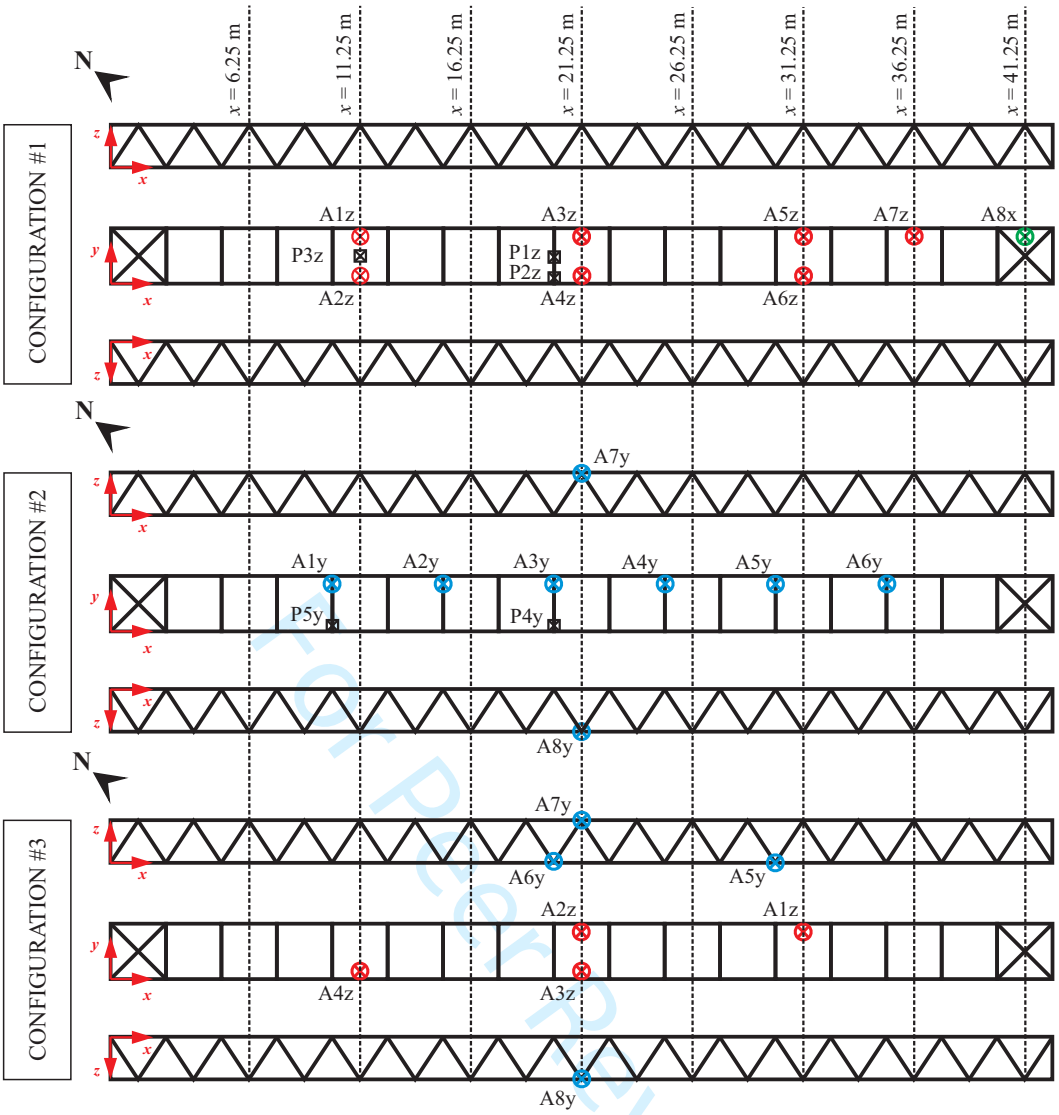

Figure 3. Main span sensor layout and excitation points in configurations #1, #2 and #3 of the experimental program. Lateral (y), vertical (z) and longitudinal (x) accelerometers are identified in the figure.

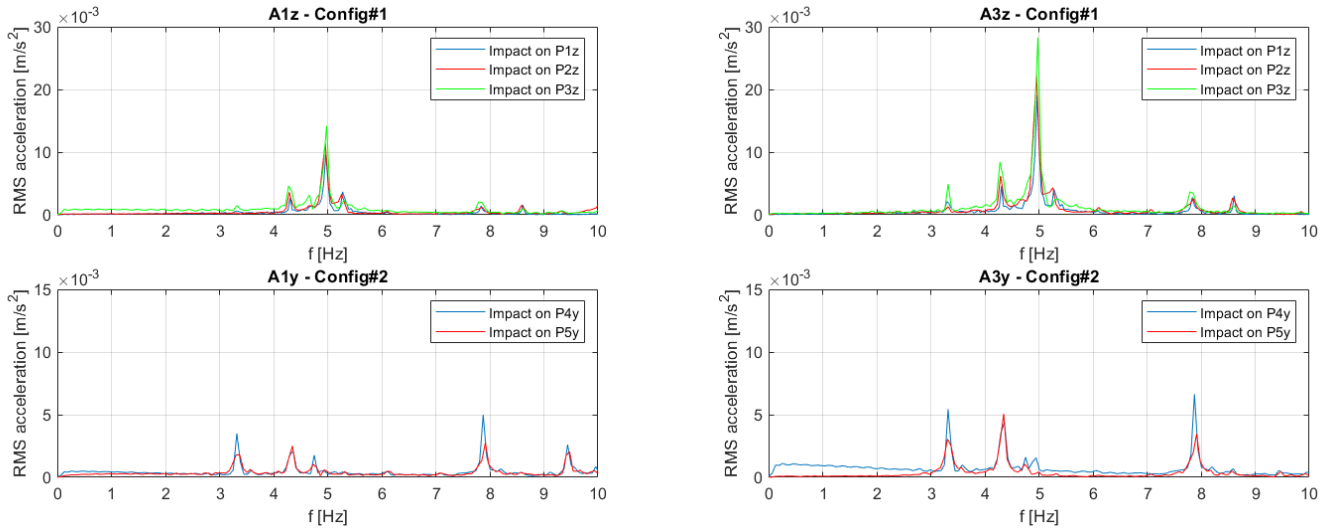

Figure 4. Response of the structure, in the frequency domain, measured during the impact tests in two accelerometers of each configuration. The RMS values from the three excitation trials are plotted.

resonance was induced on the footbridge as shown in what follows. In this section, the signals recorded during the 14 serviceability tests are analysed focusing to the acceleration comfort limits established by HiVoSS and Setra (see Fig. 1c). Tables 7 and 8 in Annex 1 show the percentage of time

with acceleration measurements within the different comfort ranges for each sensor and each test.

Regarding the pedestrian use of the bridge, quite different results have been obtained in the random walking test and in the running tests. In the random walking test with three pedestrians (Test ID #7), all measurements from the vertical accelerometers were within the maximum comfort range. This percentage was reduced to approximately 70% for the recorded lateral vibration in the two accelerometers installed at mid-span on the upper chord at both sides of the deck (A7y and A8y). No lateral vibration measurements fell within the uncomfortable class limits, and the percentage of time with lateral acceleration within the minimum comfort class was below 8.2%. The acceleration recorded during this test by the sensor showing worst comfort scores (A8y) is represented in Fig. 5, in the time and in the frequency (FFT) domains. The time signal does not exceed 0.8 m/s^2, and the frequency plot shows major contribution of the first two modes identified in Program #1 (3.32 Hz and 4.31 Hz), but also of the 8.60 Hz mode, the local truss mode identified from the impact hammer tests at one of the highest frequencies, which shows a very significant contribution to the response under pedestrian load. The peaks may not match exactly the values of the natural frequencies found in Program #1 because of a combination of factors: the experimental programs were performed in different dates and environmental conditions. Also, the recording time was not the same in boths programs (i.e. Program #2 tests records had higher frequency resolution), but the frequency differences are minor.

In the running tests (Test ID #1-4 and #8-11), the vertical vibration measurements were not fully within the maximum comfort class in many cases. The percentage of time within this comfort level ranged from 70.7 % to 99.81 %, the lowest value corresponding to the running test with only one pedestrian, at a 150 bpm pace (2.5 Hz), half of the natural frequency of the first vertical bending mode. Figure 6a shows a bar plot with the percentage of time within the different comfort classes for sensor A2z in all the tests, the one showing the worst scores in the vertical direction. The difference between the results from the tests with three pedestrians versus the corresponding ones with only one pedestrian is small. As for the lateral vibration, the percentage of time within maximum comfort level for accelerometers located at mid-span ranged between 73.15 % and 95.54 % for the one on the deck, and between 55.44 % and 68.75 % for those on the upper chords. The percentage of time with lateral vibration measurements within the uncomfortable class reached 21.29 % in accelerometer A8y for the running test at the natural frequency of the first lateral vibration mode. Again, the sensor showing worst comfort scores was A8y. From the bar plot corresponding to sensor A8y (Fig. 6b) it may be concluded that the tests performed with only one pedestrian provided more critical results than those performed with three pedestrians. The worst results were obtained for one pedestrian running at paces 195 bpm (3.25 Hz), 128 bpm (2.13 Hz) and 155 bpm (2.58 Hz), which correspond to the natural frequencies (or submultiples) of the first three vibration modes. This might be attributable to a loss of synchronisation between the three pedestrians while exciting the footbridge at specific forcing frequencies, that could be compensating the (not so high) increase in the pedestrians self-weight, which in the case of three pedestrians involves less than 2% of the main span total mass, or to additional human-human interaction effects. For a more detailed analysis, Fig. 5 shows the signal from accelerometer A8y in all tests with one pedestrian in the time and frequency domains. The time signals show that acceleration magnitudes in the running tests are higher than those observed during the random walking test. From the FFTs we can observe that the running tests at paces 3.25 Hz, 2.13 Hz and 2.5 Hz excited the first, second and third modes, respectively. The running test at 155 bpm (2.58 Hz), however, did not excite the 7.75 Hz mode, probably because the runners path was slightly closer to the deck center than what was intended, but a peak at 8.6 Hz is observed in the FFT. Further numerical analyses might bring some light into this issue. The 8.6 Hz peak is also observed as a secondary contribution in the rest of tests, especially in the running test at 150 bpm (2.5 Hz), and the random walking test, as previously mentioned. These results are contrary to the usual guidelines assumption that the maximum dynamic response in footbridges is caused by resonance of a single mode excited by the pedestrian action. Clearly the presence of close modes in the low frequency range results into their simultaneous excitation, as also observed in (12).

In the so-called *vandal* tests, the percentage of time within the maximum comfort level for the skipping and bouncing at 195 bpm pace (3.25 Hz) was close to that observed during the running tests at the same pace, both for vertical and lateral vibrations, slightly higher in some accelerometers and slightly lower in others. Interestingly, the skipping test with three pedestrians at 150 bpm pace (half of 5 Hz) provided a percentage of time with accelerations within the uncomfortable class that reached 10.6 % for vertical vibration (in A2z) and 10.5 % for lateral vibration (in A8y), as can be observed in figure 6. This skipping test provided, therefore, the highest percentage of time with accelerations within the uncomfortable class regarding vibration in the vertical direction.

Description of the numerical model

In what follows, a detailed FE numerical model of the footbridge is described. Two variants of this model are updated with the experimentally identified modal parameters later on. The model represents the three parts of the footbridge included in Fig. 7: (i) the main span, the (ii) North-West and the (iii) South-East access ramps.

The truss chords and diagonal members in the main span and ramps are modelled as Timoshenko beam elements, with a shear factor of 0.44 (31). The deck floor plates and the plates conforming the four-arm piers are modelled with 4-node quadrilateral shell elements with reduced integration and large-strain formulation. The concrete bases are modelled using eight-node solid elements with incompatible modes to avoid shear locking and reduce volumetric locking. A linear elastic material model is admitted for steel with elastic modulus, Poisson's ratio and mass density $E_s = 210$ GPa and $\mu_s = 0.3$ and $\rho_s = 7850$ kg/m^3, respectively. The same material behaviour is admitted for concrete with elastic modulus, Poisson's ratio and mass

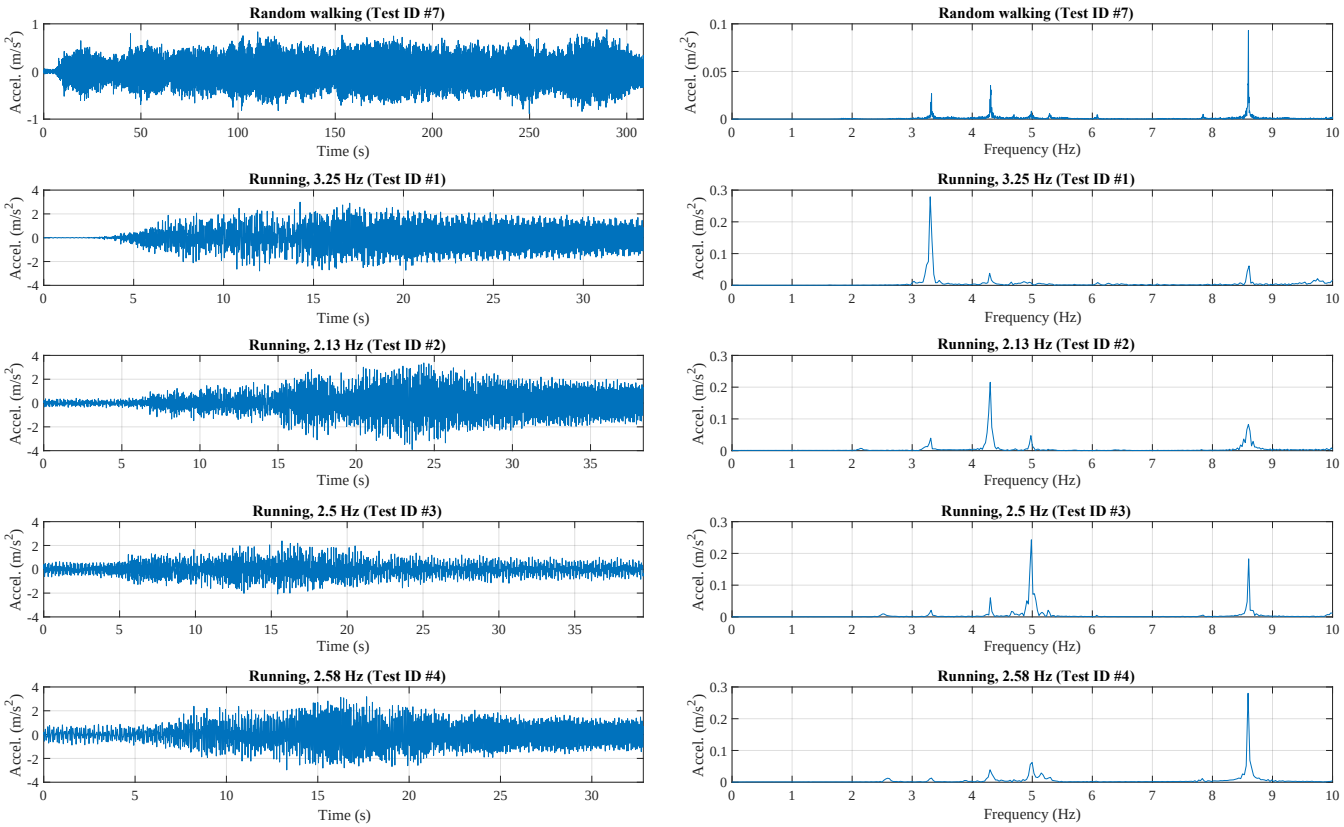

Figure 5. Acceleration signals measured in sensor A8y of Configuration #3 during the random walking and running tests with only one pedestrian, in the time and frequency (FFT) domains.

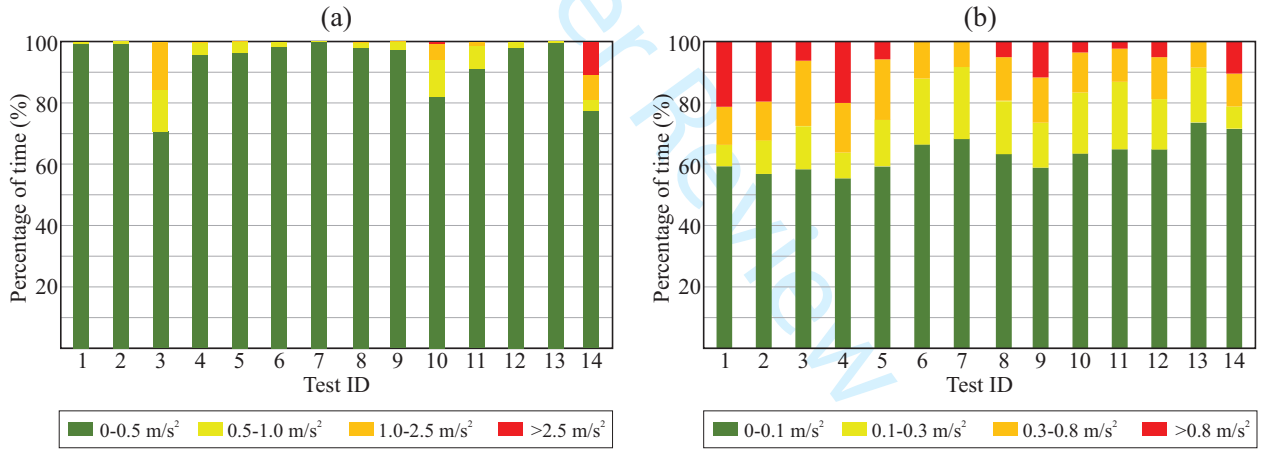

Figure 6. Percentage of time with accelerations within the different comfort classes established by European guidelines HiVoSS and SETRA during serviceability tests for accelerometers (a) A2z (vertical) and (b) A8y (lateral)

density $E_c = 33.6$ GPa and $\mu_c = 0.2$ and $\rho_c = 2300$ kg/m^3, respectively. These are nominal values prior to the updating process.

The connections between the piers four arms and the upper deck are achieved with multi-point constraints, whereas the connection between the pier bases and the concrete columns are modelled considering an embedment length of 0.5 m (see Fig. 8) and enforcing a congruent mesh.

Four different boundary conditions are specified in the FE model, which are denoted as BC1, BC2, BC3 and BC4 in Fig. 7. The nodal translations at both ends of the access ramps in contact with the ground are restricted (BC4). As for boundary conditions BC1, BC2 and BC3, rigid surfaces are defined at the bottom of the concrete bases (BC1 and BC3) and at the South-East pier lower border (BC2), the translations and rotations of these surfaces being coupled to those of three respective reference nodes placed at the center of each surface, as illustrated in Fig. 8. These reference nodes are used to specify the boundary conditions at the piers. Given the uncertainties in the definition of the substructure due to the lack of technical information available, two modelling alternatives are considered and updated in the following sections:

- Modelling alternative #1: All the translations and rotations are restricted at the reference nodes (BC1, BC2 and BC3), thus simulating a fully fixed connection of the concrete bases and of the South-East pier base to the foundations.

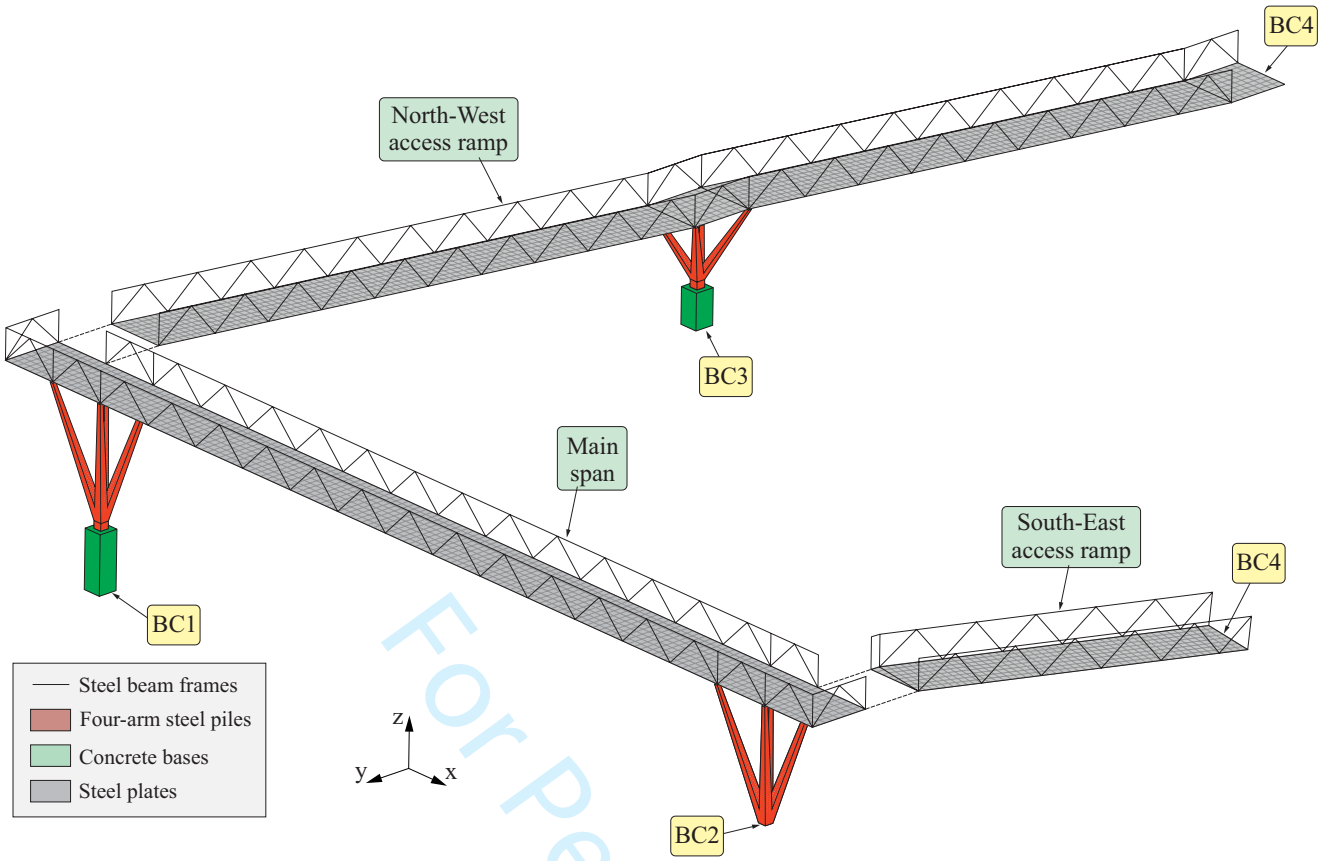

Figure 7. Overview of the numerical model

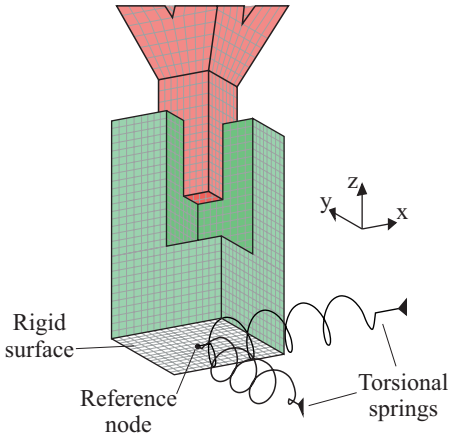

Figure 8. Model pier-to-concrete base embedment detail and definition of rigid surface, reference node and torsional springs at BC1, BC2 and BC3.

- Modelling alternative #2: All the translations are restricted at the reference nodes at BC1, BC2 and BC3, as well as the rotation about the z axis. However, the rotations with respect to x and y axes are partially restrained by torsional springs with elastic stiffnesses K_{BC1}, K_{BC2} and K_{BC3}, identical in the two directions.

Finally, natural frequencies and mode shapes are extracted using a Lanczos scheme. The modal amplitudes at the accelerometers positions are retrieved for the first modes and used in the updating procedure, described in the next section.

Model updating: pairing algorithm

In the next subsections, the numerical model is updated with the first four natural frequencies and mode-shapes identified experimentally. In order to minimize the difference between experimental and numerical results, the objective function δ is defined as:

$$\delta = \sum_{i=1}^{4} w_i \cdot F_{i,j_o} \tag{1}$$

where $i = \{1, 2, 3, 4\}$ refers to the experimental modes, w_i is the weight associated to each mode ($w_1 = 0.5$, $w_2 = 0.267$, $w_3 = 0.133$ and $w_4 = 0.1$) and F_{i,j_o} is a product that measures the degree of similarity between the experimental mode i and the paired numerical mode j_o. Prior to the application of Eq. 1, the numerical mode $j_o = \{1, .., j_{max}\}$ that is effectively paired to the experimental mode i is determined applying the algorithm shown in Fig. 9.

This algorithm starts by setting $j_o = 0$ and $F_{i,j_o} = 0$ (step **A1**). Then, the algorithm iterates through all the available numerical modes and, for each pair of experimental mode i and numerical mode j, computes the Modal Assurance Criterion ($MAC_{i,j}$) (32) and the relative difference between the experimental and numerical frequencies ($e_{i,j}$) using Eq. 2a and Eq. 2b, respectively (step **A2**).

$$MAC_{i,j} = \frac{\left(\Phi_i^{exp,T} \cdot \Phi_j^{num}\right)^2}{\left(\Phi_i^{exp,T} \cdot \Phi_i^{exp}\right) \cdot \left(\Phi_j^{num,T} \cdot \Phi_j^{num}\right)} \tag{2a}$$

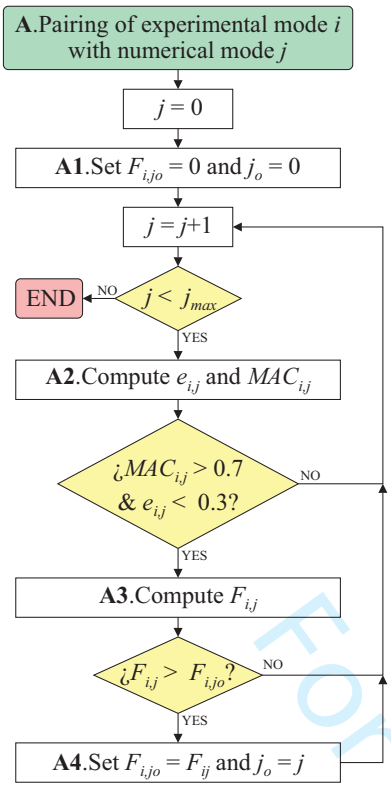

Figure 9. Pairing algorithm between experimental and numerical modes.

$$e_{i,j} = \left| \frac{f_j^{num} - f_i^{exp}}{f_i^{exp}} \right| \tag{2b}$$

Here, Φ_i^{exp} and Φ_j^{num} stand for the experimental and numerical mode vectors, respectively, and f_i^{exp} and f_j^{num} are the corresponding natural frequencies. Superscript T stands for transpose.

If the conditions $MAC_{i,j} > 0.7$ and $e_{i,j} < 0.3$ are simultaneously fulfilled, the similarity modal function $F_{i,j}$ is calculated as (step **A3**):

$$F_{i,j} = (1 - e_{i,j}) \cdot MAC_{i,j} \tag{3}$$

where $F_{i,j} = 1$ indicates a perfect experimental-numerical pairing. If the magnitude of this function is lower than the maximum value calculated in previous iterations (F_{i,j_o}), then the following numerical mode $j + i$ is assessed. On the contrary, F_{i,j_o} is set equal to $F_{i,j}$, and j_o is set to j (step **A4**). The loop is repeated until all the numerical modes are evaluated. In the end, the numerical mode j_o paired to the experimental mode i and the magnitude of the similarity function F_{i,j_o} are obtained.

Once the modes are paired and the modal similarity functions are obtained, the objective function δ is computed applying Eq. 1. Objective funtion δ provides values in the range [0,1], 1 meaning that numerical and experimental models provide identical results. Table 5 exemplifies this process for the first iteration of the model (alternative #1).

Model updating: optimisation and final results

The results shown in Tab. 5 indicate that the numerical model #1 with nominal parameters already provides a fair initial approximation of the experimental results. Nevertheless, given the aforementioned uncertainties (i.e. elastic material properties, total mass of the super-structure, thickness of the pier arm plates, foundation conditions), the model is optimised by means of a genetic algorithm (33). The function to be maximised is δ, defined as per Eq. 1. Two different optimisations are performed, where a variation of $\pm 25\%$ is allowed for the optimised variables:

- Optimisation #1: This optimisation is conducted considering modelling alternative #1. Five parameters are selected for the optimisation process: the elastic modulus and the density of the materials, steel and concrete, and the thickness of the four-arm piers cold-formed plates.
- Optimisation #2: This optimisation is conducted considering modelling alternative #2. Three additional parameters are considered, corresponding to the stiffness of the torsional springs at the supports K_{BC1}, K_{BC2} and K_{BC3}.

In Table 6 the final results of the optimisation process are included. In Optimisation #1, it is observed that the

Table 5. Pairing algorithm results for nominal case study and modelling alternative #1, where $\delta = 0.92$.

i	j	$e_{i,j}$	$MAC_{i,j}$	$F_{i,j}$	
1	1	0.10	1.00	0.90	
1	2	0.41	0.92	0.54	
1	3	0.54	0.01	0.00	
1	4	0.58	0.63	0.00	
1	5	0.72	0.10	0.00	$j_o = 1$
1	6	1.00	0.07	0.00	$F_{1,j_o} = 0.90$
1	7	1.06	0.03	0.00	
1	8	1.43	0.00	0.00	
1	9	1.45	0.27	0.00	
2	1	0.16	0.80	0.68	
2	2	0.08	0.99	0.91	
2	3	0.18	0.02	0.00	
2	4	0.21	0.31	0.00	
2	5	0.31	0.05	0.00	$j_o = 2$
2	6	0.53	0.56	0.00	$F_{2,j_o} = 0.91$
2	7	0.57	0.61	0.00	
2	8	0.65	0.03	0.00	
2	9	0.86	0.96	0.00	
3	1	0.29	0.01	0.00	
3	2	0.08	0.00	0.00	
3	3	0.00	1.00	1.00	
3	4	0.03	0.12	0.00	
3	5	0.12	0.26	0.00	$j_o = 3$
3	6	0.30	0.02	0.00	$F_{3,j_o} = 1.00$
3	7	0.34	0.08	0.00	
3	8	0.40	1.00	0.59	
3	9	0.58	0.02	0.00	
4	1	0.54	0.29	0.00	
4	2	0.41	0.10	0.00	
4	3	0.35	0.00	0.00	
4	4	0.34	0.02	0.00	
4	5	0.28	0.01	0.00	$j_o = 9$
4	6	0.16	0.09	0.00	$F_{4,j_o} = 0.93$
4	7	0.14	0.15	0.00	
4	8	0.09	0.00	0.00	
4	9	0.02	0.95	0.93	

optimisation process improves the degree of similarity between the numerical and the experimental results, especially for the first, second and fourth modes. The degree of similarity of the third mode is slightly reduced. A similar trend is observed in Optimisation #2.

Table 6. Results of the optimisation.

Parameter	Opt. #1	Opt. #2
Steel elastic modulus (GPa)	193	197
Steel density (kg/m^3)	8272	8270
Concrete elastic modulus (GPa)	27.20	30.00
Concrete density (kg/m^3)	2461	2290
Piers plate thickness (mm)	4.00	4.90
Stiffness K_{BC1} (N · m/rad 10^8)	-	3.67
Stiffness K_{BC2} (N · m/rad 10^8)	-	77.7
Stiffness K_{BC3} (N · m/rad 10^8)	-	0.31
Similarity function F_{1,j_o}	0.991	0.996
Similarity function F_{2,j_o}	0.984	0.994
Similarity function F_{3,j_o}	0.919	0.926
Similarity function F_{4,j_o}	0.966	0.964
Objective function δ	0.977	0.984

The final results of Optimisation #1 and the evolution of the algorithm itself indicate the need of reducing the stiffness of the piers to match the experimental results, with both elastic moduli and thickness of the column plates tending to implausibe low values. For this reason, the fully clamped boundary conditions at the pier bases assumed in the first model are put into question, and the second alternative allowing minimal rotations at the bases is evaluated.

From the results of Optimisation #2, the stiffness of the piers is not so drastically reduced and the optimum version of the model exhibits certain rotational flexibility at the pier bases. This specially affects BC1 and BC3, which are the supports that contribute the most to the modal shapes included in the optimisation, the foundation at the South-East pier behaving comparatively much more as a fixed support.

Moreover, both optimisations indicate that the total mass of the model is underestimated. This is consistent with the fact that some geometrical details that contribute to the mass but not to the stiffness of the footbridge have been disregarded (i.e. welds, security gratings and connection plates). Both optimisations provide a similar final mass of steel. After the optimisation, and as a consequence of the change in the density of the materials, the overall mass of the model is increased in 1461 kg: 360 kg from the concrete bases and 1101 kg from the steel parts, which matches reasonably well with the mass estimated for the disregarded material.

Finally, both optimisations provide very good objective functions (0.977 for Opt. #1 and 0.984 in the case of Opt. #2) with a certain increase of the nominal mass of the structure and close-to-nominal elastic properties. In footbridges as the one presented herein, for which the lowest natural modes exhibit an important participation of the substructure, being able to predict the supporting conditions behaviour under dynamic loads is important. This requires the detailing of the foundations which is not always available. In these cases, the experimental characterisation becomes essential to update numerical models that represent accurately the dynamic response of the structure and can be used to assess its performance under new conditions of use.

The numerical modes paired with the first four experimental modes are shown in Fig. 10. The first three experimental modes are paired with the first three numerical ones, while the forth experimental mode is paired with the fifth numerical one. The forth numerical mode corresponds to a local bending mode of the lateral trusses in the main span. The participation of the deck in this mode is small and has less interest. This mode seems to correspond to the experimental one observed at 8.56 Hz. The frequency difference is probably due to the omission of the security gratings in the model.

Finally, the maximum acceleration is determined using harmonic load models (as per section 4.5.1 in HiVoSS) for two traffic classes: very weak traffic (TC1) and weak traffic (TC2). The first one corresponds to the pedestrian density of experimental Program #2 during the random walking tests (Test ID#7), while the second represents the nowadays normal use of the structure. A harmonic analysis is performed on the numerical model that resulted from Optimisation #2, and the footbridge vertical and lateral acceleration is calculated for an excitation frequency in the vicinity of 4.25 Hz (second mode frequency), given that a null reduction coefficient is obtained for the remaining modes according to HiVoSS, which indicates a very low probability of the footfall frequency approaching the remaining natural frequencies. The modal damping identified during Program #1 for the second mode (1.09%) is considered in these analyses. In the vertical direction the maximum acceleration is predicted at the central section of the main span and remains in the maximum comfort zone both for very weak traffic (TC1) and for weak traffic (TC2), 0.09 and 0.23 m/s^2 being reached, respectively. In the lateral direction the maximum acceleration predicted takes place at mid-span in the upper chord, and falls within the medium comfort limits for very weak traffic conditions (0.14 m/s^2). For weak traffic, the maximum response crosses the limit of minimum comfort at the chord (0.39 m/s^2), which deforms laterally in the torsion mode, but not at the deck level (0.28 m/s^2). From the analyses performed it is concluded that the results obtained are consistent with the experimental response of the footbridge measured during the random walking tests. Also, the dynamic behaviour of the footbridge is adequate for weak traffic conditions, which are representative of nowadays use. However, for more intense uses it could give rise to significant vibrations at frequencies associated with walking or running, especially in the lateral direction.

Conclusions

In this paper, the dynamic performance of a light steel pedestrian footbridge is addressed. The footbridge is composed of a main steel truss span and two access ramps perpendicular to the former. The structure is elevated on three slender four-arm piers of variable hollow cross-section. Due to the structural configuration, the footbridge exhibits several modes of vibration below 10 Hz. In some of them, a relevant participation of the supports and access ramps is

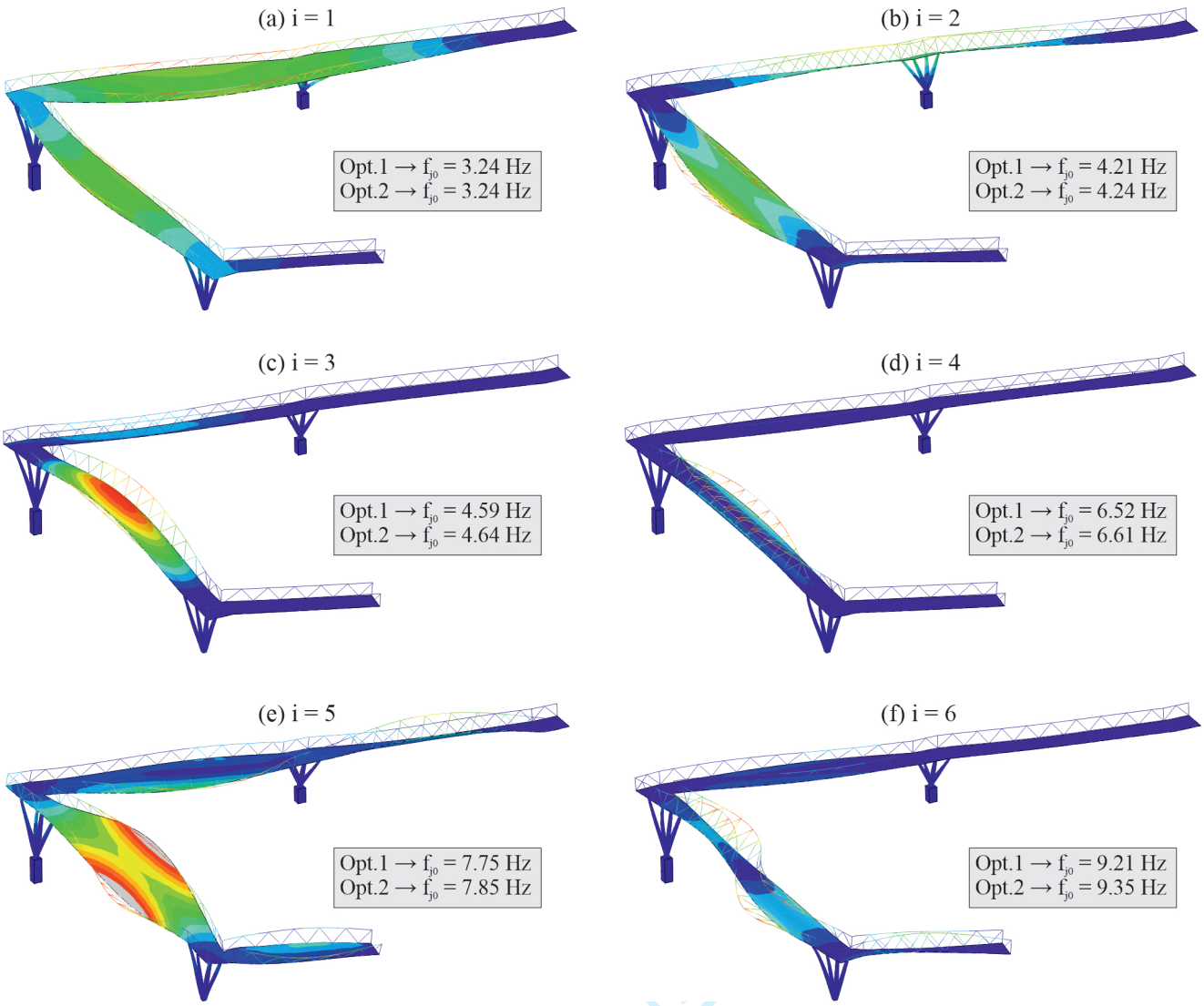

Figure 10. Mode shapes of the optimised model: modes paired with the (a) first experimental mode, (b) second experimental mode, (c) third experimental mode and (d) fourth experimental mode.

observed, leading to intricate deformed modal shapes at low frequencies.

The two main aims of the research performed are (i) to assess the vibration serviceability of the footbridge according to current codes and regulations for different pedestrian actions, including vandal hypothetical situations; and (ii) to analyse the effect of two modelling alternatives and propose a numerical model that reproduces the dynamic behaviour of the structure in the frequency range of interest with sufficient accuracy.

To this end, first, two experimental programs were performed on the bridge. In the first program the structural response was recorded under several impact hammer tests, and the modal parameters (natural frequencies, mode shapes and damping ratios) were identified. In the second experimental program, fourteen tests were performed on the footbridge to simulate various types of use by one and three pedestrians: random walking and running, bouncing and skipping at specific paces. From the experimental assessment of the vibration serviceability, the following is concluded:

- During the random walking tests with three pedestrians, representing its normal use, the recorded vertical accelerations were always within the maximum comfort class. In the lateral direction 30% of the time the accelerations were under this limit, but never fell within the minimum comfort class. In any case, the number of pedestrians considered is far from the maximum expectable occupancy of the footbridge, and more tests with a greater number of pedestrians would be advisable.
- Although the lowest natural frequencies fell within the ranges of minimum resonance risk, during synchronised pedestrian actions (running, bouncing and skipping at submultiples of the natural frequencies) the acceleration exceeded the minimum acceptable comfort limits for a considerable amount of time.
- Resonance of the first three vibration modes was induced with running paces below 3.25 Hz, which calls into question the recommendation of avoiding further dynamical analyses in case of minimum resonance risk natural frequencies.

- The presence of close modes in the low frequency range resulted into their simultaneous excitation during the serviceability tests, in opposition to the common guidelines hypothesis that the maximum expected level of vibrations in footbridges is caused by resonance of a single mode.

Second, a detailed 3D FE numerical model is implemented including the access ramps connected to the main span, the pile supports and the massive concrete short columns at the bases. In view of the pile supports influence on the low frequency modes of vibration, two modelling alternatives are envisaged: fully embedded concrete columns in the soil-foundation system and partially clamped columns, allowing a certain level of rotation at the base. The models are updated from the modal properties identified experimentally by means of an iterative genetic algorithm. From the model updating performed the following is concluded:

- Both optimisations led to an accurate representation of the real structure in terms of natural frequencies and MAC numbers of the first experimental four modes. Nevertheless, in the authors' opinion, in the model with fully fixed supports the piers need to be unrealistically flexibilised. Allowing marginal rotation capabilities to the columns base-foundation systems leads to an even better representation of the modal parameters with more realistic structural properties.
- In slender structures as the Castellón CV10 footbridge, with a relevant contribution of the substructure in the lowest modes of vibration, the idealisation of the supporting conditions under dynamic loads is important. This requires detailed information of the foundations which is not always available. In these cases, the experimental characterisation becomes essential to update numerical models that represent accurately the dynamic response, and can be used to assess the footbridge performance safely under new conditions of use.
- Finally, when the maximum acceleration is assessed numerically according to standards it is concluded that the dynamic behaviour of the footbridge is adequate for weak traffic conditions, which are representative of nowadays use. However, for more intense uses it could give rise to significant vibrations at frequencies associated with walking or running, especially in the lateral direction.

Acknowledgements

The authors would like to acknowledge the financial support provided by Universitat Jaume I under research project GACUJI/2020/11.

References

[1] Bachmann H and Ammann W. *Vibrations in structures induced by man and machines*. International Association for Bridge and Structural Engineering, 1987.

[2] Živanović S, Pavic A and Reynolds P. Vibration serviceability of footbridges under human-induced excitation: a literature review. *Journal of Sound and Vibration* 2005; 279(1): 1–74. DOI:https://doi.org/10.1016/j.jsv.2004.01.019.

[3] Stimac I. Serviceability verification of pedestrian bridges under pedestrian loading. *Tehnicki vjesnik* 2015; 22(2): 527–537. DOI:https://doi.org/10.17559/TV-20131030105641.

[4] Gimsing N and Georgakis C. *Cable supported bridges: concept and design*. John Wiley and Sons, 2012.

[5] Ingólfsson E, Georgakis C and Jönsson J. Pedestrian-induced lateral vibrations of footbridges: A literature review. *Engineering Structures* 2012; 45: 21–52. DOI:https://doi.org/10.1016/j.engstruct.2012.05.038.

[6] CEN/TC250. *Eurocode: Basis of structural design. Annex A2: Application for bridges. Final version*. European Committee for Standardization, Brussels, 2005.

[7] SETRA. *Technical guide: Footbridges. Assessment of vibrational behaviour of foot bridges under pedestrian loading*. SETRA, 2006.

[8] HiVoSS Research fund for coal and steel. *Human induced vibrations of steel structures: design of footbridges, Guideline*. RFS2-CT, 2008.

[9] IAP11. *Instrucción sobre las acciones a considerar en el proyecto de puentes de carretera*. Ministerio de Fomento, 2011.

[10] BS 5400-2:2006. *Steel, concrete and composite bridges. Specification for loads*. BSI, 2006.

[11] AASHTO. *LRFD Bridge Design Specifications*. AASHTO, 2020.

[12] Lievens K, Lombaert G, Van Nimmen K et al. Robust vibration serviceability assessment of footbridges subjected to pedestrian excitation: strategy and applications. *Engineering Structures* 2018; 171: 236–246. DOI:https://doi.org/10.1016/j.engstruct.2018.05.047.

[13] Van Nimmen K, Lombaert G, De Roeck G et al. The impact of vertical human-structure interaction on the response of footbridges to pedestrian excitation. *Journal of Sound and Vibration* 2017; 402: 104–121. DOI:https://doi.org/10.1016/j.jsv.2017.05.017.

[14] Carroll S, Owen J and Hussein M. Experimental identification of the lateral human–structure interaction mechanism and assessment of the inverted-pendulum biomechanical model. *Journal of Sound and Vibration* 2014; 333(22): 5865–5884. DOI:https://doi.org/10.1016/j.jsv.2014.06.022.

[15] Helbing D, Buzna L, Johansson A et al. Self-organized pedestrian crowd dynamics: Experiments, simulations, and design solutions. *Transportation Science* 2005; 39(1): 1–24. DOI:10.1287/trsc.1040.0108.

[16] Al-Smadi YM, Al-Rousan RZ, Laradhi AA et al. Vibration serviceability investigation of a curved footbridge. *Practice Periodical on Structural Design and Construction* 2022; 27(4): 04022040. DOI:10.1061/(ASCE)SC.1943-5576.0000714.

[17] Tadeu A, Romero A, Dias S et al. Vibration serviceability assessment of the world's longest suspended footbridge in 2020. *Structures* 2022; 44: 457–475. DOI:https://doi.org/10.1016/j.istruc.2022.08.015.

[18] Bayat E, Milone A, Tubino F et al. Vibration serviceability assessment of a historic suspension footbridge. *Buildings* 2022; 12(6). DOI:10.3390/buildings12060732.

[19] Rodríguez-Suesca A, Gutiérrez-Junco O and Hernández-Montes E. Vibration performance assessment of deteriorating footbridges: A study of tunja's public footbridges. *Engineering Structures* 2022; 256: 113997. DOI:https://doi.org/10.

1016/j.engstruct.2022.113997.

[20] Andrade A, Pimentel R, da Silva S et al. Conditions to avoid synchronization effects in lateral vibration of footbridges. *Structural Monitoring and Maintenance, an International Journal* 2022; 9: 201–220. DOI:https://doi.org/10.12989/smm.2022.9.2.201.

[21] Cuevas RG, Jiménez-Alonso JF, Martínez F et al. Assessment of the lateral vibration serviceability limit state of slender footbridges including the postlock-in behaviour. *Applied Sciences* 2020; 10(3). DOI:10.3390/app10030967.

[22] Gallegos-Calderón C, Naranjo-Pérez J, García-Palacios JH et al. Design and performance of a tuned vibration absorber for a full-scale lightweight frp pedestrian structure. *Journal of Composites for Construction* 2022; 26(6): 04022077. DOI:10.1061/(ASCE)CC.1943-5614.0001270.

[23] Saber H, Samani FS and Pellicano F. A novel nonlinear variable damping device and its application for the systems with uncertain parameters. *Proceedings of the Institution of Mechanical Engineers, Part K: Journal of Multi-body Dynamics* 2022; 236(4): 660–671. DOI:10.1177/14644193221115007.

[24] Zoltowski K, Banas A, Binczyk M et al. Control of the bridge span vibration with high coefficient passive damper. theoretical consideration and application. *Engineering Structures* 2022; 254: 113781. DOI:https://doi.org/10.1016/j.engstruct.2021.113781.

[25] Schubert Pfeil M, Diniz Varela W and de Paula Amador da Costa N. Experimental calibration of a one degree of freedom biodynamic model to simulate human walking-structure interaction. *Engineering Structures* 2022; 262: 114330. DOI:https://doi.org/10.1016/j.engstruct.2022.114330.

[26] Nelison J, Ibisevic A, Ugur H et al. Experimental and numerical dynamic properties of two timber footbridges including seasonal effects. *International Journal of Civil Engineering* 2021; 19(10): 1239–1250. DOI:10.1007/s40999-021-00624-w.

[27] Anastasopoulos D, Reynders EP, François S et al. Vibration-based monitoring of an frp footbridge with embedded fiber-bragg gratings: Influence of temperature vs. damage. *Composite Structures* 2022; 287: 115295. DOI:https://doi.org/10.1016/j.compstruct.2022.115295.

[28] CEB. *Vibration problems in structures. Practical guidelines*. CEB, 2011.

[29] UNE-EN 10219-2:2019. *Cold formed welded steel structural hollow sections - Part 2: Tolerances, dimensions and sectional properties*. 2019.

[30] UNE-EN 10025-2:2020. *Hot rolled products of structural steels - Part 2: Technical delivery conditions for non-alloy structural steels*. 2020.

[31] Cowper GR. The Shear Coefficient in Timoshenko's Beam Theory. *Journal of Applied Mechanics* 1966; 33(2): 335–340. DOI:10.1115/1.3625046.

[32] Allemang RJ. The modal assurance criterion–twenty years of use and abuse. *Sound and vibration* 2003; 37(8): 14–23.

[33] Conn AR, Gould NIM and Toint P. A globally convergent augmented lagrangian algorithm for optimization with general constraints and simple bounds. *SIAM Journal on Numerical Analysis* 1991; 28(2): 545–572. DOI:10.1137/0728030.

Annex 1

Table 7: Serviceability results. Percentages of time within the different acceleration comfort ranges according to the European guidelines HiVoSS and SETRA, for accelerometers measuring vertical vibration (A1z to A4z).

Test ID	A1z				A2z				A3z				A4z			
	0-0.5 m/s^2	0.5-1 m/s^2	1-2.5 m/s^2	> 2.5 m/s^2	0-0.5 m/s^2	0.5-1 m/s^2	1-2.5 m/s^2	> 2.5 m/s^2	0-0.5 m/s^2	0.5-1 m/s^2	1-2.5 m/s^2	> 2.5 m/s^2	0-0.5 m/s^2	0.5-1 m/s^2	1-2.5 m/s^2	> 2.5 m/s^2
1	98.77	1.23	0.00	0.00	99.40	0.60	0.00	0.00	99.81	0.19	0.00	0.00	98.99	1.01	0.00	0.00
2	99.49	0.51	0.00	0.00	99.31	0.69	0.00	0.00	99.33	0.67	0.00	0.00	99.59	0.42	0.00	0.00
3	82.62	17.17	0.22	0.00	70.70	13.77	15.53	0.00	72.95	17.60	9.44	0.00	88.44	11.54	0.03	0.00
4	98.83	1.14	0.02	0.00	95.87	4.05	0.08	0.00	96.65	3.28	0.07	0.00	99.01	0.99	0.00	0.00
5	99.79	0.21	0.00	0.00	96.34	3.60	0.06	0.00	98.08	1.89	0.03	0.00	99.87	0.13	0.00	0.00
6	100.00	0.00	0.00	0.00	98.37	1.63	0.00	0.00	99.27	0.73	0.00	0.00	100.00	0.00	0.00	0.00
7	100.00	0.00	0.00	0.00	100.00	0.00	0.00	0.00	100.00	0.00	0.00	0.00	100.00	0.00	0.00	0.00
8	98.62	1.33	0.05	0.00	98.07	1.78	0.15	0.00	99.11	0.89	0.00	0.00	99.24	0.76	0.00	0.00
9	98.67	1.28	0.04	0.00	97.51	2.37	0.12	0.00	96.92	2.95	0.13	0.00	98.67	1.32	0.01	0.00
10	93.66	5.24	1.10	0.00	82.32	11.77	5.52	0.39	84.60	11.20	4.13	0.00	95.63	3.58	0.79	0.00
11	98.03	1.92	0.06	0.00	91.27	7.54	1.19	0.00	93.73	5.81	0.47	0.00	97.83	2.13	0.05	0.00
12	99.98	0.02	0.00	0.00	98.29	1.71	0.00	0.00	97.60	2.40	0.00	0.00	99.95	0.05	0.00	0.00
13	100.00	0.00	0.00	0.00	99.60	0.40	0.00	0.00	99.88	0.12	0.00	0.00	100.00	0.00	0.00	0.00
14	81.04	4.89	12.79	1.28	77.61	3.58	8.21	10.60	78.39	3.83	9.60	0.00	81.75	6.32	11.86	0.08

Table 8: Serviceability results. Percentages of time within the different acceleration comfort ranges according to the European guidelines HiVoSS and SETRA, for accelerometers measuring lateral vibration (A5y to A8y).

Test ID	A5y				A6y				A7y				A8y			
	0-0.1 m/s^2	0.1-0.3 m/s^2	0.3-0.8 m/s^2	> 0.8 m/s^2	0-0.1 m/s^2	0.1-0.3 m/s^2	0.3-0.8 m/s^2	> 0.8 m/s^2	0-0.1 m/s^2	0.1-0.3 m/s^2	0.3-0.8 m/s^2	> 0.8 m/s^2	0-0.1 m/s^2	0.1-0.3 m/s^2	0.3-0.8 m/s^2	> 0.8 m/s^2
1	80.67	18.23	1.10	0.00	74.26	21.67	4.07	0.00	60.85	8.56	17.39	13.21	59.37	6.94	12.40	21.29
2	87.92	11.93	0.16	0.00	82.60	16.51	0.89	0.00	58.67	12.08	14.87	14.38	56.80	10.96	12.66	19.58
3	94.87	5.12	0.01	0.00	91.59	8.26	0.15	0.00	60.97	17.96	18.80	2.27	58.39	14.04	21.28	6.29
4	91.57	8.24	0.19	0.00	84.91	14.55	0.53	0.00	55.83	11.06	21.22	11.89	55.44	8.38	16.18	20.01
5	88.45	11.54	0.01	0.00	81.48	18.19	0.33	0.00	62.35	18.65	16.60	2.40	59.26	15.19	19.71	5.84
6	99.80	0.20	0.00	0.00	97.96	2.04	0.00	0.00	70.31	22.84	6.85	0.00	66.45	21.55	11.97	0.03
7	98.07	1.93	0.00	0.00	95.68	4.32	0.00	0.00	70.91	23.67	5.42	0.00	68.35	23.47	8.18	0.00
8	84.25	11.59	4.17	0.00	78.29	14.96	6.28	0.47	64.99	18.86	12.09	4.06	63.37	17.28	14.25	5.11
9	80.03	17.65	2.31	0.00	73.15	20.64	6.17	0.05	58.50	16.67	16.38	8.45	58.92	14.68	14.72	11.68
10	96.25	3.71	0.05	0.00	95.54	4.39	0.07	0.00	67.16	20.64	10.59	1.61	63.51	19.88	13.03	3.57
11	94.51	5.46	0.03	0.00	91.20	8.76	0.04	0.00	68.75	23.33	7.19	0.73	64.82	22.02	10.78	2.37
12	89.46	10.45	0.09	0.00	83.96	14.90	1.14	0.00	65.61	17.54	13.41	3.44	64.87	16.41	13.67	5.06
13	98.04	1.96	0.00	0.00	94.14	5.86	0.00	0.00	74.59	18.62	6.74	0.05	73.56	17.91	8.34	0.19
14	90.78	9.16	0.07	0.00	88.20	11.54	0.26	0.00	73.50	10.36	12.81	3.34	71.51	7.22	10.77	10.50